Metalorganic chemical vapor deposition of β-FeSi2 on β-FeSi2 seed crystals formed on Si substrates

著者	Suzuno Mitsushi, Akutsu Keiichi, Kawakami Hideki, Akiyama Kensuke, Suemasu Takashi
journal or publication title	Thin solid films
volume	519
number	24
page range	8473-8476
year	2011-10
権利	(C) 2011 Elsevier B.V. NOTICE: this is the author's version of a work that was accepted for publication in Thin solid films. Changes resulting from the publishing process, such as peer review, editing, corrections, structural formatting, and other quality control mechanisms may not be reflected in this document. Changes may have been made to this work since it was submitted for publication. A definitive version was subsequently published in PUBLICATION, VOL519, ISSUE24, 2011, DOI:10.1016/j.tsf.2011.05.029
URL	http://hdl.handle.net/2241/115897

doi: 10.1016/j.tsf.2011.05.029

Fabrication of Fe_3Si/CaF_2 heterostructures ferromagnetic resonant tunneling diode by selected-area molecular beam epitaxy

Kenji Sadakuni-Makabe [a], Mitsushi Suzuno [a], Kazunori Harada [a], Takashi Suemasu [a], Hiro Akinaga[b]

[a]*Institute of Applied Physics, University of Tsukuba, 1-1-1 Tennohdai, Tsukuba, Ibaraki 305-8573, Japan*

[b]*Nanodevice Innovation Research Center and Nanotechnology Research Institute, National Institute of Advanced Industrial Science and Technology, Tsukuba, Ibaraki 305-8568, Japan*

We have fabricated 200-nm-diameter ferromagnetic resonant tunneling diodes (FM-RTDs) using CaF_2/Fe_3Si heterostructures on Si(111) substrates, by selected-area molecular beam epitaxy (MBE) using electron-beam (EB) lithography. Clear negative differential resistances (NDRs) were observed in the current-voltage (*I-V*) characteristics at room temperature (RT). The reproducibility of the *I-V* characteristics was greatly improved, and approximately 40% of the FM-RTDs showed clear NDRs at RT.

1. Introduction

Spintronics has attracted much attention, because applications of the spin degree of freedom of electrons to semiconductor devices are expected to significantly improve their performance [1-3]. For this purpose, highly spin-polarized materials have been studied extensively as sources of spin currents. We think that the application of spin filtering effect is an alternative way to obtain spin-dependent transport. A ferromagnetic resonant tunneling diode (FM-RTD) is considered to behave as a spin filter, because spin splitting of the quantum levels in a ferromagnetic quantum well can be utilized [4-7]. We have focused on Fe_3Si/CaF_2 heterostructures because of the following reasons. First, the lattice mismatch between Fe_3Si and Si, and that between CaF_2 and Si are both relatively small, being 3.5 or 0.6%, respectively [8,9]. Thus, high-quality layered structures using CaF_2/Fe_3Si can be expected. We have developed a technique for epitaxial growth of Fe_3Si/CaF_2 multilayers on Si(111) substrates by molecular beam epitaxy (MBE) [10-12]. Second, Fe_3Si has a relatively high Curie temperature of approximately 570 ºC [13]. Third, the barrier height for electrons in Fe_3Si to tunnel through the CaF_2 barrier layer is very large (ca. 2.5 eV) [12]. Owing to this large barrier height, CaF_2/Fe_3Si FM-RTDs are expected to work as a very sharp spin filter as well as an energy filter even at room temperature (RT).

In our previous work, we fabricated 6×6 μm^2-area CaF_2 (5 nm)/Fe_3Si (4 nm)/CaF_2 (5 nm) FM-RTDs by conventional photolithography processes, and realized clear negative different resistance (NDR) with a peak-to-valley current ratio (PVCR) of nearly 1000 in the current density versus voltage (*J*-*V*) characteristics at RT [14]. The *J*–*V* characteristics were measured under the dc voltages sweeping in the upward direction. However, the reproducibility of the *J*-*V* characteristics was very poor, preventing us from doing experiments for the spin-dependent transport under external magnetic field; NDR appeared in only two RTDs out of thirty six. Such poor reproducibility was due probably to the leakage current caused by defects or pinholes in the CaF_2 barrier layers [15,16]. One way to decrease the number of defects included in the device area is the reduction of device area. In this paper, we adopted a selected-area MBE growth technique for RTD fabrication on Si(111) substrates [17], because this technique was reported to decrease the leakage current and improve the reproducibility of CaF_2/CdF_2/CaF_2 RTDs [17,18].

2. Experimental

An approximately 50-nm-thick SiO_2 layer covering 0.5 × 1 cm^2 area on a 1 × 1 cm^2 n^+-Si(111) (ρ= 0.02 Ω·cm) substrate was deposited by plasma enhanced chemical

vapor deposition at 350 ºC. The uncovered Si surface was used for *in-situ* surface monitoring by reflection high-energy electron diffraction (RHEED). Arrays of approximately 46,000 holes with 200-nm-diameters and 700-nm-periods were formed in the 150×150 μm^2 areas of the SiO_2 layer by electron-beam (EB) lithography, CH_3 dry chemical etching and O_2 plasma ashing. The oxide layers on the Si surface in the holes were removed by thermal cleaning at approximately 800 ºC in the ultrahigh vacuum. Then, the FM-RTDs of Fe_3Si (10 nm)/CaF_2 (3 nm)/Fe_3Si (5 nm)/CaF_2 (3 nm) multilayers were grown by MBE. On top of the $FeSi_2$ layer, a 3-nm-thick Fe film was deposited at 130 ºC. The growth temperatures for Fe_3Si and CaF_2 layers were 80 and 300 ºC, respectively, and the annealing temperature was 300 ºC for both materials. After the growth, we deposited 500-μm-diameter Au/Cr electrodes on the 150×150 μm^2 area to measure the averaged current-voltage characteristics, where one Au/Cr electrode contains approximately 46,000 fine RTDs. For comparison, similar Fe_3Si/CaF_2 FM-RTD structure was also grown on the bare surface of the Si(111) substrate.

3. Result and discussion

Figure 1 shows RHEED patterns taken along [1-10] azimuth of Si after the growth of (a) a Si buffer layer, (b) a CaF_2 bottom barrier layer, (c) an Fe_3Si quantum

well layer, and (d) a CaF_2 upper barrier layer. As the MBE growth proceeded, the RHEED pattern was found to be degraded; however, it can be at least stated that a double-barrier RTD structure of relatively good crystalline quality was fabricated from the bottom through the top.

Figure 2 shows the cross sections of transmission electron microscope (TEM) images taken for the FM-RTD structure grown on (a) the bare Si (111) substrate, and (b) the patterned SiO_2 layers on Si (111). Figure 2(c) shows a magnified image of a 200-nm-diameter RTD shown in Fig. 1(b). As shown by arrows in Fig. 1(a), defects or pinholes can be easily seen in the layered structure grown on the bare Si (111) surface. In contrast, those defects can't be easily found in the fine RTD as shown in Fig. 1(c), meaning that we succeeded in reducing the number of defects included in RTDs.

Figure 3(a) shows an example of *J*–*V* characteristics. A clear NDR with a PVCR of approximately 30 was observed around 4 V under forward bias conditions, where electrons are emitted from the n^+-Si into the FM-RTDs. Figure 3(b) shows the d^2J/dV^2 versus *V* plot. The peak voltages in the d^2J/dV^2-*V* plot correspond roughly to the resonant voltages [19]. The peak voltages are seen around 0.5, 2, and 4 V. Figure 3(c) shows the distribution of the resonant voltages examined for the 23 FM-RTDs, showing that the first, second, and third resonant voltages appear at approximately 0.4-0.6 V,

1.9-2.5 V, and 3.7-4.3 V. The voltage separations of approximately 1.5-2 V can be well explained by the energy separation among the three quantized levels above the Fermi level in the CaF_2 (3 nm)/Fe_3Si (5 nm)/CaF_2 (3 nm) structure, which is approximately 0.75-1eV from free-electron approximation using Tsu-Esaki formula [20]. Therefore, the peak voltages observed in the d^2J/dV^2-V characteristics can be well explained by resonant tunneling through the quantized levels, assuming that the applied voltage drops equally across the two CaF_2 barrier layers. Figure 3(d) shows the distribution in the peak voltages where NDR was observed in the J-V characteristics. NDRs were found only under forward bias conditions. Because of the very large Fermi energy (~11 eV) of Fe_3Si, it is difficult to observe NDR under reverse bias conditions. A total of 9 FM-RTDs showed clear NDRs out of 23 FM-RTDs. On the basis of these results, we concluded that the reproducibility of the J-V characteristics was improved drastically by adopting the selected-area MBE, due probably to the reduction in the number of defects included in the device area. In this work, the diameter of a fine RTD was fixed at 200 nm. It is true that we'd better investigate the device area dependence of reproducibility of the J-V characteristics. But we think that there is no need to go into details about this issue because validity of this selected-area MBE itself has been verified in Ref. 17. Our next target is to confirm the spin splitting of quantized levels in the Fe_3Si quantum well.

According to Bansil *et al*. [21], the exchange splitting of Fe_3Si is as large as approximately 0.6-1.0 eV. This value is close to the energy separation of quantized levels determined from the Fe_3Si thickness. This means that it is very difficult to confirm the existence of spin splitted quantized levels, because the voltage separation between the peak positions in the d^2J/dV^2-V characteristics, expected from the spin splitting, is close to that determined from the Fe_3Si quantum-well thickness. As to the AlAs/GaAs/AlAs RTDs with ferromagnetic p-type (Ga,Mn)As on one side, spontaneous spin splitting of ferromagnetic (Ga,Mn)As valence band was observed below the ferromagnetic transition temperature of (Ga,Mn)As [22]. Thus, we are now planning to inject spin-polarized electrons into a Si substrate from $CaF_2/Fe_3Si/CaF_2$ FM-RTDs using the non-local method [23], and then investigate the spin polarization of conducting spins [24], and compare it with that obtained for the Fe_3Si/CaF_2 tunnel junction.

4. Summary

We have successfully fabricated FM-RTDs with CaF_2/Fe_3Si heterostructures on Si(111) substrates and confirmed NDR in the *J*-*V* characteristics at RT. The PVCR of NDR in 200-nm-diameter fine FM-RTDs grown by selected-area MBE is 30. The reproducibility of the *J*-*V* characteristics was improved dramatically; NDR appeared in

nine RTDs out of twenty-three. This is due probably to the reduction in the number of defects included in the device area.

Acknowledgements

This work was supported in part by a Grant-in-Aid for Scientific Research in the Priority Area of “Creation and Control of Spin Current” (No. 19048029, MEXT), the NanoProcessing Partnership Platform (NPPP) at AIST and NIMS-CNN Nano Foundries at NIMS in Tsukuba, Japan. The authors would also thank Dr. N. Ikeda of NIMS for his help with the EB lithography, Prof. M. Isshiki and Dr. M. Uchikoshi of the Tohoku University for supplying us high-purity 5N Fe sources.

Reference

[1] S. Matsunaga, J. Hayakawa, S. Ikeda, K. Miura, H. Hasegawa, T. Endoh, H. Ohno, and T. Hanyu: Appl. Phys. Express **1** (2008) 091301.

[2] I. Appelbaum, B. Huang, and D. J. Monsma: Nature **447** (2007) 295.

[3] H. K. Mst, M. Shahjahan, K. Sawada, and M. Ishida: Physica E **36** (2007) 123.

[4] T. Hayashi and M. Tanaka: J. Appl. Phys. **87** (2000) 4673.

[5] S. Ohya, P. N. Hai, Y. Mizuno, and M. Tanaka: Phys. Rev. B **75** (2007) 155328.

[6] S. Ohya, I. Muneta, and M. Tanaka: Appl. Phys. Lett. **96** (2010) 052505.

[7] K. Gananasekar and K. Navaneethakrishnan: Physica E **28** (2005) 328.

[8] K. Kataoka, K. Hattori, Y. Miyatake, and H. Daimon: Phys. Rev. B **74** (2006) 155406.

[9] K. Nath and A. B. Anderson: Phys. Rev. B **38** (1988) 388264.

[10] K. Kobayashi, T. Sunohara, M. Umada, H. Yanagihara, E. Kita, and T. Suemasu: Thin Solid Films **508** (2006) 78.

[11] T. Harianto, K. Kobayashi, T. Suemasu, and H. Akinaga: Jpn. J. Appl. Phys. **46** (2007) L904.

[12] T. Harianto, K. Sadakuni, H. Akinaga, and T. Suemasu: Jpn. J. Appl. Phys. **74** (2008) 6310T.

[13] J. Waliszewski, L. Dobrzynski, A. Malinowski, D. Satula, K. Szmanski, W. Prandl, Th. Brückel, and O. Schärpf: J. Magn. Magn. Mater. **132** (1994) 349.

[14] K. Sadakuni, T. Harianto, H. Akinaga, and T. Suemasu: Appl. Phys. Express **2** (2009) 063006.

[15] J. Wollschläger: Appl. Phys. A **75** (2002) 155.

[16] Y. Horio and S. Satoh: J. Surf. Sci. Soc. Jpn. **22** (2001) 552.

[17] T. Kanazawa, A. Morosawa, R. Fujii, T. Wada, Y. Suzuki, M. Watanabe, and M. Asada: Jpn. J. Appl. Phys. **46** (2007) 3388.

[18] M. Maeda, N. Matsudo, S. Watanabe, and K. Tsutsui: J. Cryst. Growth **285** (2005) 572.

[19] M. Tsuchiya, and H. Sakaki: Jpn. J. Appl. Phys. **30** (1991) 1164.

[20] R. Tsu and L. Esaki: Appl. Phys. Lett. **22** (1973) 562.

[21] A. Bansil, S. Kaprzyk, P. E. Mijnarends, and J. Toboła: Phys. Rev. B 60 (1999) 13396.

[22] H. Ohno, N. Akiba, F. Matsukura, A. Shen, K. Ohtani, and Y. Ohno: Appl. Phys. Lett. **73** (1998) 363.

[23] T. Uhrmann, T. Dimopoulos, H. Brucki, V. K. Lazarov, A. Kohn, U. Paschen, S. Weyers, L. Bar, and M. Ruhrig: J. Appl. Phys. **103** (2008) 063709.

[24] S. Takahashi and S. Maekawa: Phys. Rev. B **67** (2003) 052409.

Figure 1 RHEED patterns taken along [1-10] azimuth of Si after the each growth of (a) a Si buffer layer, (b) a CaF_2 bottom barrier layer, (c) an Fe_3Si quantum well layer, and (d) a CaF_2 upper barrier layer.

Figure 2 TEM cross sections of FM-RTDs grown on (a) the bare Si(111) substrate and (b) the patterned SiO_2 on the Si(111). Arrows indicate the positions of defects. (c) Magnified TEM image of a 200-nm-diameter fine RTD shown in Fig. 2(b).

Figure 3 Typical examples of (a) *J*-*V* and (b) d^2J/dV^2-*V* characteristics of the FM-RTD measured at RT which the bias voltage was applied to the surface with respect to the Si substrate. The distributions of (c) the peak voltage in the d^2J/dV^2-*V* characteristics and (d) the NDR voltage in the *J*-*V* characteristics.

(a)

(b)

(c)

(d)

Figure 1

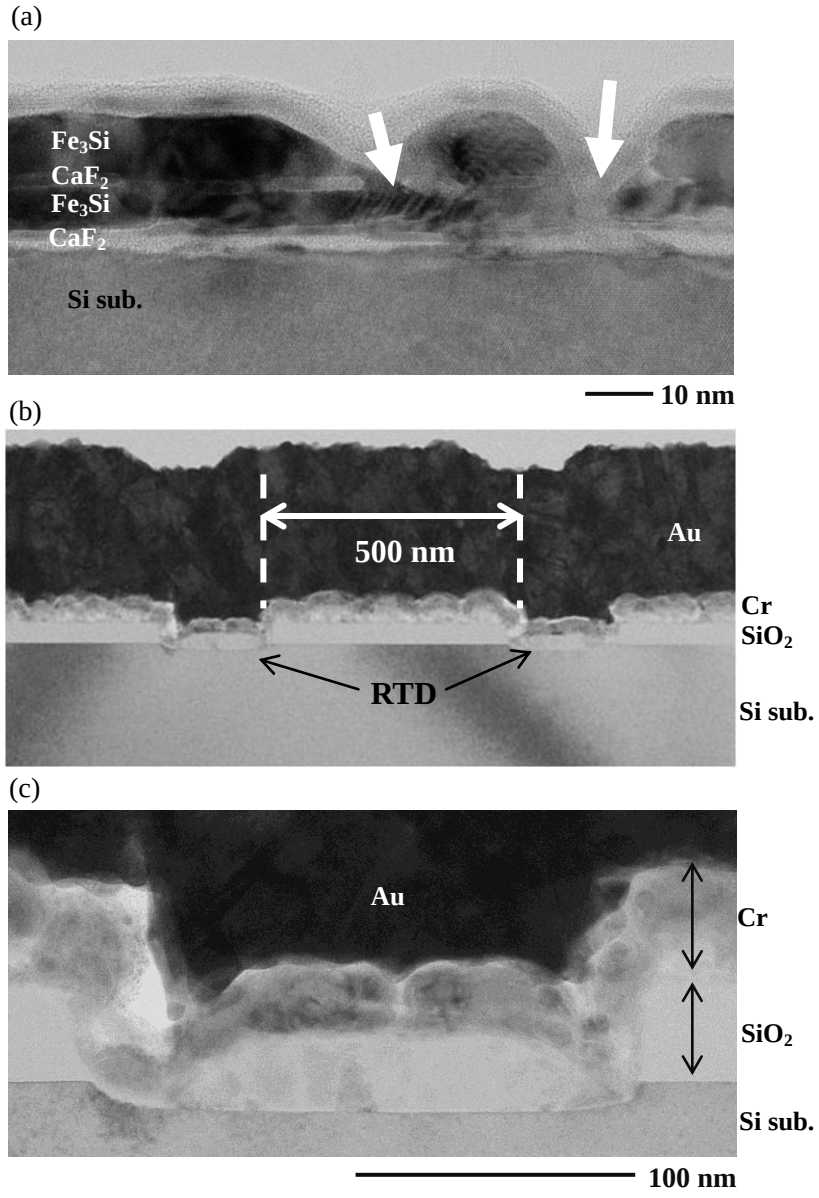
(a)
Fe3Si
CaF2
Fe3Si
CaF2
Si sub.
10 nm
(b)
500 nm
Au
Cr
SiO2
RTD
Si sub.
(c)
Au
Cr
SiO2
Si sub.
100 nm

Figure 2

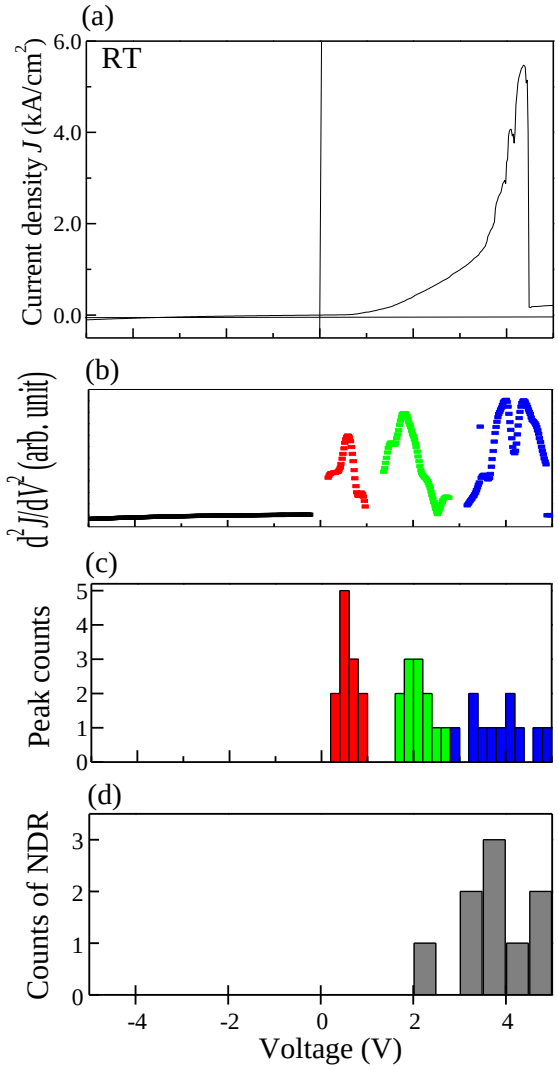
(a)
RT
Current density J (kA/cm2)
6.0
4.0
2.0
0.0
(b)
d2J/dV2 (arb. unit)
(c)
Peak counts
5
4
3
2
1
0
(d)
Counts of NDR
3
2
1
0
-4
-2
0
2
4
Voltage (V)

Figure 3